

Making Contrastive Learning Robust to Shortcuts

Tianhong Li^{1,*} Lijie Fan^{1,*} Yuan Yuan¹ Hao He¹ Yonglong Tian¹
 Rogerio Feris² Piotr Indyk¹ Dina Katabi¹

¹MIT CSAIL, ²MIT-IBM Watson AI Lab

Abstract

Contrastive learning is one of the fastest growing research areas in machine learning due to its ability to learn useful representations without labeled data. However, contrastive learning is susceptible to shortcuts – i.e., it may learn shortcut features irrelevant to the task of interest, and discard relevant information. Past work has addressed this limitation via hand-crafted data augmentations that eliminate the shortcut. But, manually crafted augmentations do not work across all datasets and tasks. Further, data augmentations fail in addressing shortcuts in multi-attribute classification when one attribute acts as a shortcut around other attributes. In this paper, we analyze the objective function of contrastive learning and formally prove that it is vulnerable to shortcuts. We then present reconstructive contrastive learning (RCL), a framework for learning unsupervised representations that are robust to shortcuts. The key idea is to force the learned representation to reconstruct the input, which naturally counters potential shortcuts. Extensive experiments verify that RCL is highly robust to shortcuts and outperforms state-of-the-art contrastive learning methods on a variety of datasets and tasks.

Introduction

The area of unsupervised or self-supervised representation learning is growing rapidly (He et al. 2020; Doersch, Gupta, and Efros 2015; Ye et al. 2019; Hjelm et al. 2018; Grill et al. 2020; Bachman, Hjelm, and Buchwalter 2019; Zhuang, Zhai, and Yamins 2019; Misra and Maaten 2020; Han, Xie, and Zisserman 2020). It refers to learning data representations that capture potential labels of interest, and doing so without human supervision. Contrastive learning is increasingly considered as a standard and highly competitive method for unsupervised representation learning. Features learned with this method have been shown to generalize well to downstream tasks, and in some cases surpass the performance of supervised models (Oord, Li, and Vinyals 2018; Caron et al. 2020; Tschannen et al. 2019; Chen et al. 2020a,b,c).

Contrastive learning learns representations by contrasting positive samples against negative samples. During training, a data sample is chosen as an anchor (e.g., an image); positive samples are chosen as different augmented versions of the anchor (e.g., randomly cropping and color distorting the

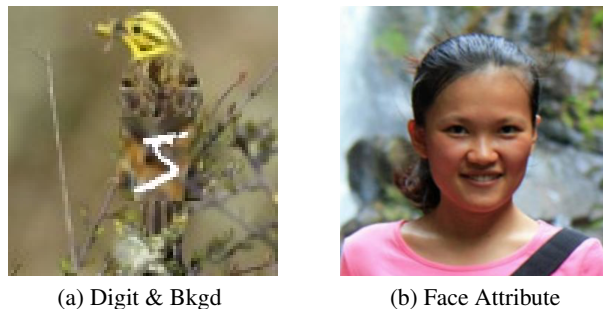


Figure 1: (a) In Colorful-MNIST (Tian et al. 2020), the input has two types of information: digit and background object. But contrastive learning methods focus on the background object and ignore the digit. (b) Each image in FairFace (Kärkkäinen and Joo 2019) has multiple attributes such as age, gender, ethnicity, etc. Existing contrastive learning methods focus on ethnicity and partially ignore other attributes.

image), whereas negative samples come from other samples in the dataset.

Yet contrastive learning is vulnerable to shortcuts – i.e., if simple features are contrastive enough to separate positive samples from negative samples, contrastive learning might learn such simple (or simpler) features even if irrelevant to the tasks of interest, and ignore other more relevant features. For example, the authors of (Chen et al. 2020a) show that color distribution can be a shortcut to distinguish patches cropped from the same image, from patches from different images; yet such feature is not useful for object classification. Past work addresses this problem by designing handcrafted data augmentations to break such shortcuts, so that the network may learn the relevant information (He et al. 2020; Chen et al. 2020a,b,c; Chen and Li 2020).

However, in many scenarios it is hard to design augmentations that remove shortcuts. For example, the authors of (Tian et al. 2020) highlight the scenario in Fig. 1 (a), where each image shows a digit (from MNIST) on a randomly chosen background object (from STL-10). They show that features related to background objects can create a shortcut that prevents contrastive learning from learning features related to digits. It is unclear how to design augmentations to learn features useful for digit classification, while keeping good performance on background object classification. A similar problem exists in the task of human face attribute classification, where

*Indicates equal contribution.

each face image can be used in multiple downstream tasks including gender, age, and ethnicity classification (Fig. 1 (b)), but the features learned by contrastive learning can be biased to only one of the attributes (e.g., ethnicity) and show poor performance on other attributes (gender and age) as shown in the experiments section. In this case, it is hard to come up with data augmentations that eliminate the shortcut attribute without harming the corresponding classification task. Moreover, as machine learning keeps expanding to new modalities it becomes increasingly difficult to design handcrafted data augmentations because many new modalities are hard to directly interpret by humans (e.g., acceleration from wearable devices), or the interpretation requires domain experts (e.g., medical data).

In this paper, we first theoretically analyze the reason why contrastive learning is vulnerable to shortcuts, and prove that learning a shortcut could lead to a saddle point or a local minimum of the infoNCE loss, whose value is very close to that of the global minimum. Based on this theoretical observation, we propose reconstructive contrastive learning (RCL), a framework that avoids shortcuts. The key idea underlying RCL is to learn representations using contrastive and reconstructive learning simultaneously. We use the term reconstructive learning to refer to tasks that force the representation to reconstruct the input, such as inpainting, colorization, or autoencoding. Such tasks counter the effect of shortcuts because they force the learned features to retain the information in the input. Once combined with reconstructive learning, contrastive learning ensures that all useful features (not just the shortcut features) are closely mapped in the embedding space for positive samples, and stay distant for negative samples. Thus, reconstructive learning maximizes the useful information in the representation, whereas contrastive learning orders the information in the embedding space to make it easy for a simple classifier to slice the embedding space to satisfy a desired task.

We evaluate RCL and compare it with state-of-the-art contrastive learning baselines on four different datasets: ImageNet, MPII (Andriluka et al. 2014), Colorful-MNIST (Tian et al. 2020), and FairFace (Kärkkäinen and Joo 2019). For all tasks, RCL achieves superior performance and outperforms the state-of-the-art baselines by large margins, demonstrating its robustness against shortcuts and its ability to learn general features for different downstream tasks.

The paper makes the following contributions:

- It gives a theoretical explanation to why contrastive learning is vulnerable to shortcuts by proving that the global minimum of the infoNCE loss at a lower feature dimension can be a local minimum or a saddle point of the infoNCE loss at a higher feature dimension.
- It introduces RCL, a self-supervised learning framework that integrates contrastive and reconstructive learning to automatically avoid shortcuts and provide a representation that supports multiple different downstream tasks.
- It empirically shows that SOTA contrastive learning baselines (e.g., SimCLR, MoCo, and BOYD) perform poorly in the presence of shortcuts and RCL outperforms these baselines on a variety of tasks including object recognition, pose estimation, and face attribute classification.

Related Work

(a) Unsupervised Contrastive Representation Learning:

Early work on unsupervised representation learning has focused on designing pretext tasks and training the network to predict their pseudo labels. Such tasks include solving jigsaw puzzles (Noroozi and Favaro 2016), restoring a missing patch in the input (Pathak et al. 2016), or predicting image rotation (Gidaris, Singh, and Komodakis 2018). However, pretext tasks have to be handcrafted, and the generality of their representations is typically limited (Chen et al. 2020a).

Hence, researchers have recently focused on contrastive learning, which emerged as a competitive and systematic method for learning effective representations without human supervision. The learned features generalize well to downstream tasks, outperform representations learned through pretext tasks, and even surpass the performance of supervised models on some tasks (Chen et al. 2020a,b,c; He et al. 2020). Multiple successful contrastive learning frameworks have been proposed, which typically differ in the way they sample negative pairs. To name a few, SimCLR (Chen et al. 2020a) uses a large batch size, and samples negative pairs within each batch. The momentum-contrastive approach (MoCo) (He et al. 2020) leverages a moving-average encoder and a queue to generate negative samples on the fly during training. Contrastive-Multiview-Coding (Tian, Krishnan, and Isola 2019) maintains a memory-bank to store features and generate negative samples. Some recent methods, like BYOL, do not rely on negative pairs (Chen and He 2020; Grill et al. 2020). Instead, they use two neural networks that learn from each other to boost performance.

Past work has also reported problems with contrastive learning. The authors of (Chen et al. 2020a) showed that color distribution can be a shortcut and proposed to break this shortcut through color-distortion data augmentation. Further, the authors of (Tian et al. 2020) noted that when the data includes multiple types of semantics, one type may produce a shortcut that prevents contrastive learning from learning effective features of other semantics (as in Figure 1(b) where the background object information can be a shortcut that prevents learning features related to digits). They proposed a solution that learns contrastive views suitable for the desired downstream task. While they share our goal of supporting different downstream tasks, their method requires supervision since they learn their contrastive views from labeled data. In contrast, our representation learning is completely unsupervised.

Another related work is contrastive-predictive-coding (CPC) (Oord, Li, and Vinyals 2018; Hénaff et al. 2019). CPC has some similarities with RCL in that it has a predictive task that aims to reconstruct missing information. However, CPC aims to reconstruct the features of a future frame, while RCL reconstructs the raw input data. As a result, the representation learned by CPC is not forced to contain necessary information to reconstruct the input, making it susceptible to shortcuts, just like other contrastive learning methods.

(b) Autoencoders (AE): The family of auto-encoders provides a popular framework for self-supervised representation learning using a reconstructive loss (Hinton and Salakhutdinov 2006; Pu et al. 2016; Vincent et al. 2008). It trains

an encoder to generate low-dimensional latent codes that could reconstruct the entire high-dimensional inputs. There are many types of AEs, such as denoising auto-encoders (Vincent et al. 2008), which corrupt the input and let the latent codes reconstruct it, and variational auto-encoders (Pu et al. 2016), which force the latent codes to follow a prior distribution. RCL can be viewed as a special variant of the denoising auto-encoder that forces the latent codes to have a ‘contrastive’ property regularized by a contrastive loss. As a result, the latent codes, are good not only for reconstructing the input, but also for downstream classification tasks.

(c) Combination of Reconstructive and Contrastive Loss: Several concurrent papers published on Arxiv also used a combination of reconstructive and contrastive loss (Dippel, Vogler, and Höhne 2021; Jiang et al. 2020). However, none of them explore the potential of this combination to solve the shortcut problem, or provides a theoretical analysis of shortcuts. This paper is the first to demonstrate that the combination of contrastive and reconstructive loss can be used to avoid shortcuts and learn general representations that support multiple downstream tasks.

Analysis: explaining shortcuts

In this section, we provide a theoretical explanation of why contrastive learning is vulnerable to shortcuts.

Let $X = \{x_i\}_{i=1}^n$ be the set of the data points. We use λ_{ij} to indicate whether a data pair x_i and x_j is positive or negative. Specifically, $\lambda_{ij} = 1$ indicates a positive pair while $\lambda_{ij} = 0$ indicates a negative pair. Let $Z = \{z_i\}_{i=1}^n$, where $z_i = f(x_i) = (z_i^1, \dots, z_i^d) \in \mathbb{S}^{d-1}$, denote the learned features on the hypersphere, generated by the neural network f . We consider the following empirical asymptotics of the infoNCE contrastive learning objective function introduced in (Wang and Isola 2020).

Definition 1 (Empirical infoNCE asymptotics).

$$\mathcal{E}_{\text{limNCE}}(Z; X, \tau, d) \triangleq -\frac{1}{\tau n^2} \sum_{ij} \lambda_{ij} z_i^\top z_j + \frac{1}{n} \sum_i \log \left(\frac{1}{n} \sum_j e^{z_i^\top z_j / \tau} \right)$$

We are going to connect the landscape of empirical infoNCE asymptotics in the low dimension to that in the high dimension. We start by defining a *lifting operator* that maps a low dimensional vector to a higher dimension.

Definition 2 (Lifting operator). A lifting operator \mathcal{T}_σ parameterized by an indexing function σ maps a d_1 -dimensional vector to dimension d_2 ($d_2 > d_1$). Its parameter σ is a permutation of length d_2 . Given a d_1 -dimensional vector z , the lifting operator maps it to a d_2 -dimensional vector $\tilde{z} = \mathcal{T}_\sigma(z)$ by the following rules: $\tilde{z}^t = z^{\sigma(t)}$ if $\sigma(t) \leq d_1$, otherwise $\tilde{z}^t = 0$.

With a slight abuse of the notation, we allow the lifting operator to map a set of low dimensional vectors to higher dimension, i.e. $\mathcal{T}_\sigma(\{z_i\}) = \{\mathcal{T}_\sigma(z_i)\}$. We further allow the lifting operator to map a function f of lower dimension to

higher dimension, i.e., $\mathcal{T}_\sigma(f)(z) = \mathcal{T}_\sigma(f(z))$. Note that \mathcal{T}_σ is a linear operator. We highlight several useful properties of \mathcal{T}_σ :

Lemma 1 (Value Invariance). *The value of the empirical infoNCE asymptotics is invariant under the lifting operation. Formally, consider any lifting operator \mathcal{T}_σ from the dimension d_1 to the dimension d_2 . We have*

$$\mathcal{E}_{\text{limNCE}}(\mathcal{T}_\sigma(Z); X, \tau, d_2) = \mathcal{E}_{\text{limNCE}}(Z; X, \tau, d_1)$$

Proof. Following the definition of \mathcal{T}_σ , $\forall z_i, z_j, z_i^\top z_j = \mathcal{T}_\sigma(z_i)^\top \mathcal{T}_\sigma(z_j)$. Therefore, $\mathcal{E}_{\text{limNCE}}(\mathcal{T}_\sigma(Z); X, \tau, d_2) = \mathcal{E}_{\text{limNCE}}(Z; X, \tau, d_1)$. \square

Lemma 2 (Gradient Equivariance). *The gradient of the empirical infoNCE asymptotics is equivariant under the lifting operation. Formally, consider any lifting operator \mathcal{T}_σ from the dimension d_1 to the dimension d_2 . We have*

$$\nabla_{\tilde{z}_k} \mathcal{E}_{\text{limNCE}}(\mathcal{T}_\sigma(Z); X, \tau, d_2) = \mathcal{T}_\sigma(\nabla_{z_k} \mathcal{E}_{\text{limNCE}}(Z; X, \tau, d_1))$$

Proof.

$$\begin{aligned} & \nabla_{\tilde{z}_k} \mathcal{E}_{\text{limNCE}}(Z; X, \tau, d_1) \\ & \triangleq \nabla_{z_k} \left(-\frac{1}{\tau n^2} \sum_{ij} \lambda_{ij} z_i^\top z_j + \frac{1}{n} \sum_i \log \left(\frac{1}{n} \sum_j e^{z_i^\top z_j / \tau} \right) \right) \\ & = -\frac{1}{\tau n^2} \left(\sum_{i \neq k} \lambda_{ki} z_i + \sum_{i \neq k} \lambda_{ik} z_i + 2\lambda_{kk} z_k \right) \\ & \quad + \frac{1}{\tau n} \frac{2z_k e^{z_k^\top z_k / \tau} + \sum_{j \neq k} z_j e^{z_k^\top z_j / \tau}}{\sum_j e^{z_k^\top z_j / \tau}} + \frac{1}{\tau n} \sum_{i \neq k} \frac{z_i e^{z_i^\top z_k / \tau}}{\sum_j e^{z_i^\top z_j / \tau}} \\ & = -\frac{1}{\tau n^2} \left(\sum_i \lambda_{ki} z_i + \sum_i \lambda_{ik} z_i \right) \\ & \quad + \frac{1}{\tau n} \frac{z_k e^{z_k^\top z_k / \tau} + \sum_j z_j e^{z_k^\top z_j / \tau}}{\sum_j e^{z_k^\top z_j / \tau}} + \frac{1}{\tau n} \sum_{i \neq k} \frac{z_i e^{z_i^\top z_k / \tau}}{\sum_j e^{z_i^\top z_j / \tau}}. \end{aligned}$$

Since \mathcal{T}_σ is a linear operator,

$$\begin{aligned} & \mathcal{T}_\sigma(\nabla_{z_k} \mathcal{E}_{\text{limNCE}}(Z; X, \tau, d_1)) \\ & = -\frac{1}{\tau n^2} \left(\sum_i \lambda_{ki} \tilde{z}_i + \sum_i \lambda_{ik} \tilde{z}_i \right) \\ & \quad + \frac{1}{\tau n} \frac{\tilde{z}_k e^{\tilde{z}_k^\top \tilde{z}_k / \tau} + \sum_j \tilde{z}_j e^{\tilde{z}_k^\top \tilde{z}_j / \tau}}{\sum_j e^{\tilde{z}_k^\top \tilde{z}_j / \tau}} + \frac{1}{\tau n} \sum_{i \neq k} \frac{\tilde{z}_i e^{\tilde{z}_i^\top \tilde{z}_k / \tau}}{\sum_j e^{\tilde{z}_i^\top \tilde{z}_j / \tau}} \\ & = -\frac{1}{\tau n^2} \left(\sum_i \lambda_{ki} \tilde{z}_i + \sum_i \lambda_{ik} \tilde{z}_i \right) \\ & \quad + \frac{1}{\tau n} \frac{\tilde{z}_k e^{\tilde{z}_k^\top \tilde{z}_k / \tau} + \sum_j \tilde{z}_j e^{\tilde{z}_k^\top \tilde{z}_j / \tau}}{\sum_j e^{\tilde{z}_k^\top \tilde{z}_j / \tau}} + \frac{1}{\tau n} \sum_{i \neq k} \frac{\tilde{z}_i e^{\tilde{z}_i^\top \tilde{z}_k / \tau}}{\sum_j e^{\tilde{z}_i^\top \tilde{z}_j / \tau}} \\ & = \nabla_{\tilde{z}_k} \mathcal{E}_{\text{limNCE}}(\mathcal{T}_\sigma(Z); X, \tau, d_2) \end{aligned}$$

where $\tilde{z}_k = \mathcal{T}_\sigma(z_k)$. The second equality comes from the fact that $\forall z_i, z_j, z_i^\top z_j =$

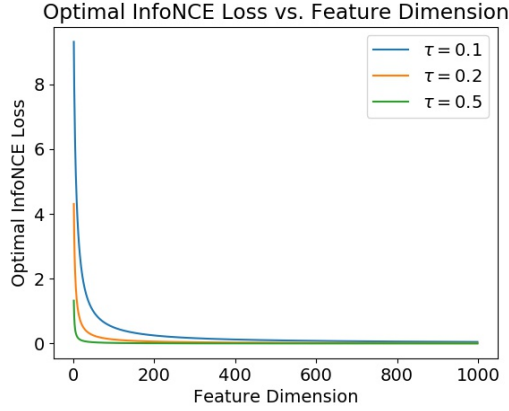


Figure 2: Optimal infoNCE loss vs. different output feature dimension d and temperature τ .

$\mathcal{T}_\sigma(z_i)^\top \mathcal{T}_\sigma(z_j)$. Thus $\nabla_{z_k} \mathcal{E}_{\text{limNCE}}(\mathcal{T}_\sigma(Z); X, \tau, d_2)$ equals $\mathcal{T}_\sigma(\nabla_{z_k} \mathcal{E}_{\text{limNCE}}(Z; X, \tau, d_1))$, for all $z_k \in Z$. \square

Corollary 1. For any lifting operator \mathcal{T}_σ , if $\hat{Z} = \{\hat{z}_i\}$ is a stationary point of $\mathcal{E}_{\text{limNCE}}(Z; X, \tau, d_1)$, then $\mathcal{T}_\sigma(\hat{Z})$ is a stationary point of $\mathcal{E}_{\text{limNCE}}(Z; X, \tau, d_2)$.

Proof. The proof is in the supplemental material. \square

Corollary 2. For any lifting operator \mathcal{T}_σ , if $\hat{Z} = \{\hat{z}_i\}$ is a global minimum of $\mathcal{E}_{\text{limNCE}}(Z; X, \tau, d_1)$ with a positive definite Hessian matrix, then $\mathcal{T}_\sigma(\hat{Z})$ is a saddle point or a local minimum of $\mathcal{E}_{\text{limNCE}}(Z; X, \tau, d_2)$.

Proof. The proof is in the supplemental material. \square

With Corollary 4, we can explain why contrastive learning can suffer from shortcuts. Suppose f is a network that achieves the global minimum of $\mathcal{E}_{\text{limNCE}}(Z; X, \tau, d_1)$. When d_1 is relatively small (e.g., < 200 for images), f must lose some information about the input, i.e., learn shortcuts. From Corollary 4, $\mathcal{T}_\sigma(f)$ is a saddle point or a local minimum of $\mathcal{E}_{\text{limNCE}}(Z; X, \tau, d_2)$ where $d_2 > d_1$ and $\mathcal{T}_\sigma(f)$ carries no more information than f . Therefore, for any dimension $d > 1$, there exists saddle point/local minimum of $\mathcal{E}_{\text{limNCE}}(Z; X, \tau, d)$ which corresponds to a shortcut.

Furthermore, the value of the aforementioned saddle point/local minimum of $\mathcal{E}_{\text{limNCE}}(Z; X, \tau, d)$ is quite close to that of the global minimum. This is because the optimal value of $\mathcal{E}_{\text{limNCE}}(Z; X, \tau, d)$ converges quickly as d increases. Figure 2 shows the curve of $\log_0 F_1(\cdot; d; \frac{1}{4\tau^2})$, which is the optimal value of the infoNCE loss (Wang, Liu, and Yu 2020). As shown in the figure, the curve essentially converges when $d > 200$. Therefore, $\mathcal{T}_\sigma(f)$ can be a saddle point/local minimum of $\mathcal{E}_{\text{limNCE}}(Z; X, \tau, d_2)$, and its value can also be quite close to that of the global minimum, hence making it hard to escape from such a saddle point or local minimum. So effectively one can achieve a value pretty close to the global minimum simply by learning a shortcut, and stay at that saddle point being unable to escape.

Reconstructive Contrastive Learning (RCL)

Reconstructive contrastive learning (RCL) is a framework for self-supervised representation learning. It aims to learn representations that are robust to shortcuts, and capable of supporting multiple diverse downstream tasks. RCL aims to provide these properties without knowing a priori the potential shortcuts or the downstream tasks.

The key idea underlying RCL is as follows: Shortcuts are harmful because they cause the features to lose important information that was available in the input. Thus, to counter shortcuts, RCL uses a reconstruction loss to ensure that the representation can restore the input, i.e., the features have the information available at the input. Yet, keeping all information in the features is not enough; the input already has all information. By adding a contrastive loss, RCL reorganizes the information in the feature space to make it amenable to downstream classification, i.e., samples that have similar attributes/objects are closer to each other than samples that have different attributes/objects. Figure 3 shows the RCL framework which has two branches: a contrastive branch and a reconstructive branch.

(a) Contrastive Branch: The contrastive branch is illustrated in the orange box in Figure 3. Here, we use SimCLR as an example to demonstrate the basic idea. However, this contrastive branch can be easily adapted to any contrastive learning method such as CPC, MoCo, and BYOL. For each image, we first generate a pair of positive samples by using two random augmentations τ_1 and τ_2 , then we forward the two augmented inputs separately to the encoder E , parameterized by θ and a multi-layer nonlinear projection head H parameterized by h to get the latent representations z_1 and z_2 for these two positive samples. We use the commonly used InfoNCE loss (Chen et al. 2020a) as the contrastive loss \mathcal{L}_c . Namely, for a batch of N different input images $x_i, i = 1, \dots, N$,

$$\mathcal{L}_c = - \sum_{i=1}^N \log \sum_{k=1}^{2N} \frac{\exp(\text{sim}(z_{2i}, z_{2i+1})/t)}{\sum_{k=1}^{2N} \mathbb{1}_{k \neq 2i} \exp(\text{sim}(z_{2i}, z_k)/t)},$$

where $\text{sim}(u, v) = u^\top v / (\|u\|_2 \|v\|_2)$ denotes the dot product between the normalized u and v (i.e., cosine similarity), $t \in \mathbb{R}^+$ is a scalar temperature parameter, and z_{2i}, z_{2i+1} are the encoded features of positive pairs generated from x_i , i.e., $z_{2i} = H_h(E_\theta(\tau_1(x_i)))$ and $z_{2i+1} = H_h(E_\theta(\tau_2(x_i)))$.

(b) Reconstructive Branch: To choose a proper reconstructive task, we need to consider two aspects: its ability to summarize and abstract the input, and its applicability to different datasets and tasks. In fact, many self-supervised learning tasks, such as Auto-encoder, Colorization and Inpainting, are reconstructive since they all aim to restore the input. But, those tasks do not have the same ability to both retain and abstract information. For example, inpainting is a stronger reconstructive task than autoencoding in terms of its ability to both abstract and retain information. Thus, although both of them would help in strengthening contrastive learning against shortcuts, inpainting is likely to provide more gains.

Another issue to consider is the applicability of the chosen task to various datasets. For example, colorization is

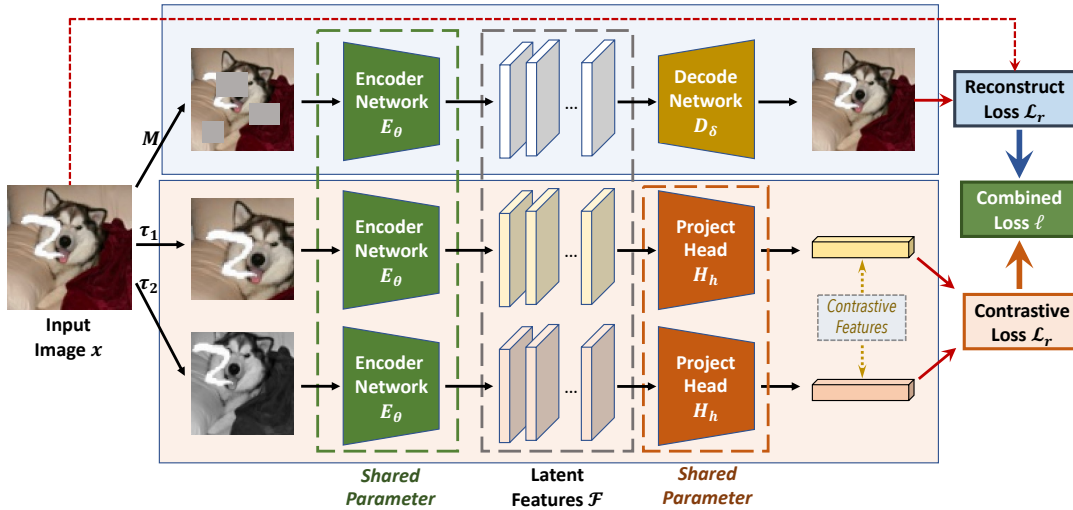


Figure 3: Illustration of the RCL framework. RCL has two branches: 1) a reconstructive branch, illustrated in the blue box, which ensures that the representation has enough information to restore missing patches in the input, and 2) a contrastive branch, illustrated in the orange box, which ensures that the representation keeps positive samples close to each other and away from negative samples.

applicable only to colorful RGB datasets, but not to grey-scale datasets such as MNIST or medical image datasets. In contrast, a task like inpainting is easier to translate across different datasets.

Given the above considerations, we adopt inpainting as the default reconstructive task. In the supplemental material, we compare various reconstructive tasks and show that while they all improve performance, inpainting delivers higher gains.

Figure 3 shows how RCL uses the inpainting task, where given an input image x , we first randomly mask several patches to get the masked input $M(x)$. Then the masked input is passed through an encoder network E with parameter θ , and a decoder network D , with parameter δ , to obtain the reconstruction result $D_\delta(E_\theta(M(x)))$. The reconstruction loss \mathcal{L}_r is defined as the reconstruction error between the original input x and the reconstructed one $D_\delta(E_\theta(M(x)))$:

$$\mathcal{L}_r = ||D_\delta(E_\theta(M(x))) - x||_2.$$

(c) Training Procedure: We have empirically found that it is better to train the model in two phases. In the first phase, only the reconstructive branch is trained. In the second phase, both branches are trained together. In this latter case, the overall training loss is the combination of the reconstruction loss and the contrastive loss, i.e., $\mathcal{L} = \mathcal{L}_c + \lambda \cdot \mathcal{L}_r$. We set $\lambda = 10$ for all experiments. We also include results with different λ in the supplemental material.

(d) RCL Avoids Shortcuts: With a combination of the reconstruction loss and the contrastive loss, RCL is capable of escaping the aforementioned local minimum/saddle points of infoNCE loss where only partial semantics are learned. This is because learning only a part of the semantics can result in very high reconstruction loss. For example, if the network learns only semantics related to the background object but ignores the digit (Figure 3), all pixels related to the digit are likely to be reconstructed incorrectly, introducing large gradients towards learning information about the digits and thus escape the saddle point.

Experiments

Baselines. We use state-of-the-art contrastive learning methods as baselines, including SimCLR (Chen et al. 2020a), MoCo (Chen et al. 2020c), CPC (Hénaff et al. 2019) and BYOL (Grill et al. 2020). The same network structure, batch size, and training epochs are used for all baselines and RCL’s contrastive branch. For the contrastive branch of RCL, we apply the same training scheme as MoCo.

Datasets. We experiment with the following datasets:

- **ImageNet** ImageNet (Deng et al. 2009) is a widely used image classification benchmark which contains 1.28M images in 1000 different categories. It is a standard benchmark to evaluate self-supervised learning methods (Chen et al. 2020c,a; Grill et al. 2020).
- **MPII** MPII (Andriluka et al. 2014) is one of the most common datasets for the task of human pose estimation. It contains images of everyday human activities.
- **FairFace** FairFace (Kärkkäinen and Joo 2019) is a face attribute classification dataset, where each image contains multiple semantics including gender, age, and ethnicity.
- **Colorful-MNIST** This is a synthetic dataset used by (Tian et al. 2020) to highlight the shortcut problem. It is constructed by assigning each digit from MNIST a background object image selected randomly from STL-10. It supports two downstream tasks: digit and background classification.

Results

We report the main results for all datasets. The experiment setup, training details and hyper-parameter settings are provided in the supplemental material along with additional results.

ImageNet. Table 1 compares RCL with the contrastive learning baselines on the task of object classification under different data augmentations. Here, we compare RCL with SimCLR and MoCo since they use the same set of data

Table 1: Performance on ImageNet with progressive removal of data augmentations for different self-supervised learning techniques. The baseline corresponds to the original set of augmentations used in SimCLR and MoCo: random flip, random resized crop, color distortion, and random Gaussian blur.

(a) ImageNet TOP-1 accuracy and its DROP w.r.t. inclusion of all augmentations.									
Method	Reconstruct		SimCLR		MoCo		RCL(ours)		IMPROVE
METRIC	TOP-1	DROP	TOP-1	DROP	TOP-1	DROP	TOP-1	DROP	
Baseline	43.7	/	67.9	/	71.1	/	71.0	/	-0.1
Remove flip	43.4	-0.3	67.3	-0.6	70.6	-0.5	70.8	-0.2	+0.2
Remove blur	43.6	-0.1	65.2	-2.7	69.7	-1.4	70.6	-0.4	+0.9
Crop color only	43.2	-0.5	64.2	-3.7	69.5	-1.6	70.1	-0.9	+0.6
Remove color distort	43.5	-0.2	45.7	-22.2	60.4	-10.7	65.9	-5.1	+5.5
Crop blur only	42.8	-0.9	41.7	-26.2	59.8	-11.3	65.1	-5.9	+5.3
Crop flip only	43.3	-0.4	40.2	-27.7	59.4	-11.7	64.6	-6.4	+5.2
Crop only	42.7	-1.0	40.3	-27.6	59.0	-12.1	64.1	-6.9	+5.1

(b) ImageNet TOP-5 accuracy and its DROP w.r.t. inclusion of all augmentations.									
Method	Reconstruct		SimCLR		MoCo		RCL(ours)		IMPROVE
METRIC	TOP-5	DROP	TOP-5	DROP	TOP-5	DROP	TOP-5	DROP	
Baseline	68.3	/	88.5	/	90.1	/	90.0	/	-0.1
Remove flip	67.9	-0.4	88.2	-0.3	89.9	-0.2	89.9	-0.1	+0.0
Remove blur	68.1	-0.2	86.6	-1.9	89.7	-0.4	89.8	-0.2	+0.1
Crop color only	67.8	-0.5	86.2	-2.3	89.6	-0.5	89.7	-0.3	+0.1
Remove color distort	68.0	-0.3	70.6	-17.9	84.2	-5.9	88.3	-1.7	+4.1
Crop blur only	67.4	-0.9	66.4	-22.1	83.1	-7.0	88.0	-2.0	+4.9
Crop flip only	67.7	-0.6	64.8	-23.7	82.0	-8.1	87.7	-2.3	+5.7
Crop only	67.4	-0.9	64.8	-23.7	81.6	-8.5	87.6	-2.4	+6.0

Table 2: Performance on MPII for the downstream task of human pose estimation. ↑ indicates the larger the value, the better the performance.

METRIC		Head	Shoulder	Elbow	Wrist	Hip	Knee	Ankle	PCKh
FIXED FEATURE EXTRACTOR	SimCLR	78.4	74.6	56.7	45.2	61.8	51.3	47.1	60.8
	MoCo	79.2	75.1	57.4	45.9	62.4	52.0	47.6	61.4
	CPC	78.0	74.3	56.0	44.8	61.2	51.4	46.5	60.3
	BYOL	79.1	75.0	57.1	46.0	62.4	52.2	47.7	61.4
	RCL (ours)	85.7	78.8	61.7	51.3	64.4	55.6	49.2	65.1
	IMPROVEMENTS	+6.5	+3.7	+4.3	+5.3	+2.0	+3.4	+1.5	+3.7
FINE- TUNING	SimCLR	96.2	94.7	87.3	81.2	87.5	81.0	77.2	87.1
	MoCo	95.9	94.7	87.5	81.6	87.4	81.7	76.9	87.2
	CPC	96.0	94.5	87.0	81.1	87.3	80.8	77.0	87.0
	BYOL	96.2	94.8	87.5	81.4	87.6	81.5	77.0	87.2
	RCL (ours)	96.3	94.9	88.1	82.3	87.9	82.8	77.8	87.8
	IMPROVEMENTS	+0.1	+0.1	+0.6	+0.7	+0.3	+1.1	+0.6	+0.6
SUPERVISED		96.3	95.1	87.9	82.2	87.8	82.7	77.8	87.7

augmentations. The results show that with fewer data augmentations, the accuracy of the contrastive learning baselines drops quickly due to shortcuts. For example, removing the color distortion augmentation significantly degrades the performance of the baseline approaches, as color distribution is known to be a strong shortcut of contrastive learning. In contrast, RCL is significantly more robust. For example, with only random cropping, RCL’s Top-1 accuracy drops by only 6.9 whereas the Top-1 accuracy of SimCLR drops by 27.6 and the Top-1 accuracy of MoCo drops by 12.1. We also compare RCL with a reconstructive baseline (Pathak et al. 2016). For the reconstructive baseline, though the model is not sensitive to different augmentations, the best performance is not comparable to contrastive learning, indicating reconstructive learning alone is not enough to learn fine-grained representations from images.

MPII. We use RCL and the contrastive learning baselines to learn representations from MPII, and evaluate them on the task of pose estimation. Table 9 shows that RCL improves the average PCKh (the standard metric for pose estimation) over the strongest contrastive baseline by 3.7 and achieves even higher gains on important keypoints such as Head and Wrist. This is because contrastive learning is likely to focus on shortcuts irrelevant to the downstream task, such as clothes and appearances.

FairFace. Table 10 compares the contrastive learning baselines to RCL on the task of face-attribute classification. The results show how contrastive learning struggles with multi-attribute classification. Specifically, the performance of the contrastive learning baselines on ethnicity classification is close to supervised learning of that attribute (62% vs. 69%). However, their results on age and gender classifications are

Table 3: Performance on FairFace with different unsupervised learning methods. The models are evaluated on downstream tasks of age, gender and ethnicity classification.

METRIC		AGE CLS ACC. (%)	GENDER CLS ACC. (%)	ETHN. CLS ACC. (%)
FIXED FEATURE EXTRACTOR	SimCLR	43.9	78.1	61.7
	MoCo	44.5	78.6	61.9
	CPC	43.5	76.2	61.0
	BYOL	44.3	78.6	62.3
	RCL (ours)	50.0	87.2	61.2
IMPROVEMENT		+5.7	+8.6	-1.1
FINE- TUNING	SimCLR	54.3	91.1	69.1
	MoCo	54.7	91.3	69.2
	CPC	54.2	91.0	68.8
	BYOL	54.6	91.5	69.3
	RCL (ours)	55.3	92.3	69.0
IMPROVEMENT		+0.6	+0.8	-0.3
SUPERVISED on AGE		55.5	78.8	45.1
SUPERVISED on GENDER		43.3	92.5	45.4
SUPERVISED on ETHN.		42.1	76.8	69.4
SUPERVISED on ALL		54.8	91.9	68.8

Table 4: Performance on Colorful-MNIST under different unsupervised methods. The models are evaluated on the downstream tasks of digit classification and background object classification.

METRIC		DIGIT CLS ACC. (%)	BKGD CLS ACC. (%)
FIXED FEATURE EXTRACTOR	SimCLR	14.9	47.3
	MoCo	15.7	48.5
	CPC	15.8	35.2
	BYOL	15.5	49.0
	RCL (ours)	88.3	46.5
IMPROVEMENT		+72.5	-2.5
FINE- TUNING	SimCLR	92.4	54.8
	MoCo	92.7	54.9
	CPC	92.3	54.7
	BYOL	92.7	54.9
	RCL (ours)	93.3	54.7
IMPROVEMENT		+0.6	-0.2
SUPERVISED on DIGIT		96.1	11.4
SUPERVISED on BKGD		12.9	56.7
SUPERVISED on DIGIT & BKGD		93.0	54.5

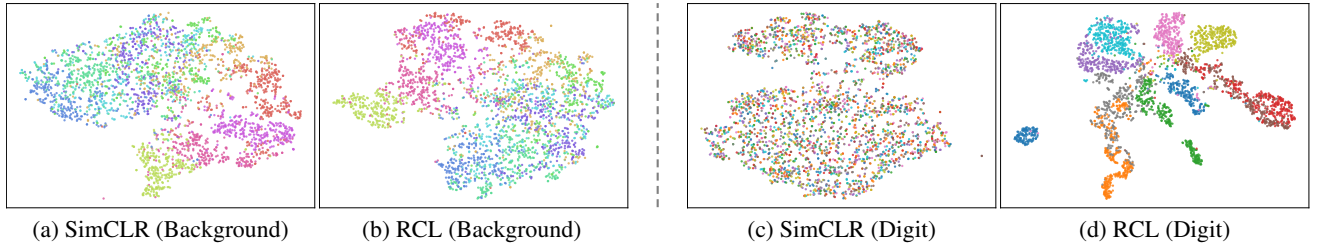


Figure 4: Visualization of latent features learned using different approaches on Colorful-MNIST dataset. The color of the left two figures corresponds to background object labels, and the color of the right two figures corresponds to the digit label.

significantly worse than supervised learning of those attributes (44% and 78% vs. 54% and 91%). This indicates that ethnicity acts as a shortcut for contrastive learning. This shortcut is partial since there are dependencies in how ethnicity manifests itself across age and gender. In contrast, RCL is much more robust to such shortcuts, and its performance results on age and gender classifications are much closer to those of fully-supervised classification of those attributes.

Colorful-MNIST. We use this dataset to further investigate how contrastive learning performs on multi-attribute classification. Recall that each image in this dataset contains a digit from MNIST on a randomly selected background object from the STL-10. We investigate whether the learned representation supports both digit and background classifications. Table 11 shows that the contrastive learning baselines learn only the task of background classification, and fail to learn a representation relevant to digit classification. This shows that information related to the background act as a shortcut preventing contrastive learning from capturing digit-relevant features. Note that the performance gap on digit classification between contrastive learning and supervised learning is very large (the accuracy is 15% vs. 93%). This is much larger than the gap we saw on FairFace because the information related to digit and background are totally independent, whereas features related to ethnicity, age, and gender have a

significant overlap. In contrast, the representation learned by RCL achieves very good accuracy on both background and digit classifications.

Figure 4 provides a t-SNE visualization (Van der Maaten and Hinton 2008) of the learned features for SimCLR and RCL. The figure shows how reconstructive learning complement contrastive learning. Comparing Figures 4(c) and 4(d) reveals that RCL’s reconstructive branch allows it to capture information about digits that is lost in SimCLR.

Conclusion

In this paper, we introduce reconstructive contrastive learning (RCL), a novel framework for making unsupervised contrastive learning more robust and allow it to preserve useful information in the presence of shortcuts. We theoretically analyze the reason why contrastive learning is vulnerable to shortcuts, and show that the reconstructive loss can help avoid shortcuts and preserve useful information. Extensive empirical results on a variety of datasets and tasks show that RCL is effective at addressing the shortcut problem. We believe that RCL provides an important step forward toward making self-supervised learning more robust and providing richer self-supervised representations that support multi-attribute classifications and generalize well across diverse tasks.

References

- Andriluka, M.; Pishchulin, L.; Gehler, P.; and Schiele, B. 2014. 2d human pose estimation: New benchmark and state of the art analysis. In *Proceedings of the IEEE Conference on computer vision and Pattern Recognition*, 3686–3693.
- Bachman, P.; Hjelm, R. D.; and Buchwalter, W. 2019. Learning representations by maximizing mutual information across views. *arXiv preprint arXiv:1906.00910*.
- Caron, M.; Misra, I.; Mairal, J.; Goyal, P.; Bojanowski, P.; and Joulin, A. 2020. Unsupervised learning of visual features by contrasting cluster assignments. *arXiv preprint arXiv:2006.09882*.
- Chen, T.; Kornblith, S.; Norouzi, M.; and Hinton, G. 2020a. A simple framework for contrastive learning of visual representations. *arXiv preprint arXiv:2002.05709*.
- Chen, T.; Kornblith, S.; Swersky, K.; Norouzi, M.; and Hinton, G. E. 2020b. Big self-supervised models are strong semi-supervised learners. *Advances in Neural Information Processing Systems*, 33.
- Chen, T.; and Li, L. 2020. Intriguing Properties of Contrastive Losses. *arXiv preprint arXiv:2011.02803*.
- Chen, X.; Fan, H.; Girshick, R.; and He, K. 2020c. Improved baselines with momentum contrastive learning. *arXiv preprint arXiv:2003.04297*.
- Chen, X.; and He, K. 2020. Exploring Simple Siamese Representation Learning. *arXiv preprint arXiv:2011.10566*.
- Deng, J.; Dong, W.; Socher, R.; Li, L.-J.; Li, K.; and Fei-Fei, L. 2009. Imagenet: A large-scale hierarchical image database. In *2009 IEEE conference on computer vision and pattern recognition*, 248–255. Ieee.
- Dippel, J.; Vogler, S.; and Höhne, J. 2021. Towards Fine-grained Visual Representations by Combining Contrastive Learning with Image Reconstruction and Attention-weighted Pooling. *arXiv preprint arXiv:2104.04323*.
- Doersch, C.; Gupta, A.; and Efros, A. A. 2015. Unsupervised visual representation learning by context prediction. In *Proceedings of the IEEE international conference on computer vision*, 1422–1430.
- Gidaris, S.; Singh, P.; and Komodakis, N. 2018. Unsupervised representation learning by predicting image rotations. *arXiv preprint arXiv:1803.07728*.
- Grill, J.-B.; Strub, F.; Altché, F.; Tallec, C.; Richemond, P. H.; Buchatskaya, E.; Doersch, C.; Pires, B. A.; Guo, Z. D.; Azar, M. G.; et al. 2020. Bootstrap your own latent: A new approach to self-supervised learning. *arXiv preprint arXiv:2006.07733*.
- Han, T.; Xie, W.; and Zisserman, A. 2020. Memory-augmented dense predictive coding for video representation learning. *arXiv preprint arXiv:2008.01065*.
- He, K.; Fan, H.; Wu, Y.; Xie, S.; and Girshick, R. 2020. Momentum contrast for unsupervised visual representation learning. In *Proceedings of the IEEE/CVF Conference on Computer Vision and Pattern Recognition*, 9729–9738.
- Hénaff, O. J.; Srinivas, A.; De Fauw, J.; Razavi, A.; Doersch, C.; Eslami, S.; and Oord, A. v. d. 2019. Data-efficient image recognition with contrastive predictive coding. *arXiv preprint arXiv:1905.09272*.
- Hinton, G. E.; and Salakhutdinov, R. R. 2006. Reducing the dimensionality of data with neural networks. *science*, 313(5786): 504–507.
- Hjelm, R. D.; Fedorov, A.; Lavoie-Marchildon, S.; Grewal, K.; Bachman, P.; Trischler, A.; and Bengio, Y. 2018. Learning deep representations by mutual information estimation and maximization. *arXiv preprint arXiv:1808.06670*.
- Jiang, D.; Li, W.; Cao, M.; Zhang, R.; Zou, W.; Han, K.; and Li, X. 2020. Speech SIMCLR: Combining Contrastive and Reconstruction Objective for Self-supervised Speech Representation Learning. *arXiv preprint arXiv:2010.13991*.
- Kärkkäinen, K.; and Joo, J. 2019. Fairface: Face attribute dataset for balanced race, gender, and age. *arXiv preprint arXiv:1908.04913*.
- Misra, I.; and Maaten, L. v. d. 2020. Self-supervised learning of pretext-invariant representations. In *Proceedings of the IEEE/CVF Conference on Computer Vision and Pattern Recognition*, 6707–6717.
- Noroozi, M.; and Favaro, P. 2016. Unsupervised learning of visual representations by solving jigsaw puzzles. In *European Conference on Computer Vision*, 69–84. Springer.
- Oord, A. v. d.; Li, Y.; and Vinyals, O. 2018. Representation learning with contrastive predictive coding. *arXiv preprint arXiv:1807.03748*.
- Pathak, D.; Krahenbuhl, P.; Donahue, J.; Darrell, T.; and Efros, A. A. 2016. Context encoders: Feature learning by inpainting. In *Proceedings of the IEEE conference on computer vision and pattern recognition*, 2536–2544.
- Pu, Y.; Gan, Z.; Henao, R.; Yuan, X.; Li, C.; Stevens, A.; and Carin, L. 2016. Variational autoencoder for deep learning of images, labels and captions. *arXiv preprint arXiv:1609.08976*.
- Tian, Y.; Krishnan, D.; and Isola, P. 2019. Contrastive multiview coding. *arXiv preprint arXiv:1906.05849*.
- Tian, Y.; Sun, C.; Poole, B.; Krishnan, D.; Schmid, C.; and Isola, P. 2020. What makes for good views for contrastive learning. *arXiv preprint arXiv:2005.10243*.
- Tschannen, M.; Djolonga, J.; Rubenstein, P. K.; Gelly, S.; and Lucic, M. 2019. On mutual information maximization for representation learning. *arXiv preprint arXiv:1907.13625*.
- Van der Maaten, L.; and Hinton, G. 2008. Visualizing data using t-SNE. *Journal of machine learning research*, 9(11).
- Vincent, P.; Larochelle, H.; Bengio, Y.; and Manzagol, P.-A. 2008. Extracting and composing robust features with denoising autoencoders. In *Proceedings of the 25th international conference on Machine learning*, 1096–1103.
- Wang, T.; and Isola, P. 2020. Understanding contrastive representation learning through alignment and uniformity on the hypersphere. In *International Conference on Machine Learning*, 9929–9939. PMLR.
- Wang, X.; Liu, Z.; and Yu, S. X. 2020. Unsupervised Feature Learning by Cross-Level Discrimination between Instances and Groups. *arXiv preprint arXiv:2008.03813*.
- Xiao, B.; Wu, H.; and Wei, Y. 2018. Simple baselines for human pose estimation and tracking. In *Proceedings of the European conference on computer vision (ECCV)*, 466–481.
- Ye, M.; Zhang, X.; Yuen, P. C.; and Chang, S.-F. 2019. Unsupervised embedding learning via invariant and spreading instance feature. In *Proceedings of the IEEE Conference on computer vision and pattern recognition*, 6210–6219.
- Zhang, R.; Isola, P.; and Efros, A. A. 2016. Colorful image colorization. In *European conference on computer vision*, 649–666. Springer.
- Zhuang, C.; Zhai, A. L.; and Yamins, D. 2019. Local aggregation for unsupervised learning of visual embeddings. In *Proceedings of the IEEE/CVF International Conference on Computer Vision*, 6002–6012.

Appendix A: Additional Results

In this section, we provide additional results to better understand the good practices for applying RCL.

Table 5: Comparison of different reconstructive tasks for RCL’s reconstructive branch. The table shows the performance of RCL on Colorful-MNIST with different reconstructive tasks in its reconstructive branch for the fixed feature encoder setting. Colorization achieves good performance on background classification, but bad performance on digit classification since the MNIST digits have no RGB information. Inpainting achieves the best performance among these reconstructive tasks.

Recon. Tasks	Colorful-MNIST	
	DIGIT CLS ACC. (%)	BKGD CLS ACC. (%)
No Recon.	15.7	48.5
Colorization	63.9	47.0
Autoencoder	65.6	42.9
Inpainting	88.3	46.5

Comparison of Different Reconstructive Tasks for RCL’s Reconstructive Branch: In RCL, we choose the inpainting task for the reconstructive branch. However, other reconstructive tasks can be potentially used for the reconstructive branch. In this section, we evaluate the performance of RCL with different reconstructive tasks including inpainting, auto-encoder and colorization (Zhang, Isola, and Efros 2016). Table 5 shows RCL’s performance using different reconstructive task on Colorful-MNIST under the fixed feature extractor setting. As shown in the table, all reconstructive tasks significantly reduce errors in comparison to using contrastive learning without any reconstruction task. The table also shows that inpainting compares favorably to other reconstructive tasks and achieves good performance on both downstream tasks. Hence, we use inpainting as the default reconstructive task in RCL.

Table 6: Performance of MoCo on Colorful-MNIST without masking augmentation (fixed feature encoder setting). The results demonstrate that simply adding masking as a data augmentation does not achieve similar improvements as RCL.

Recon. Tasks	Colorful-MNIST	
	DIGIT CLS ACC. (%)	BKGD CLS ACC. (%)
MoCo w/o masking	15.7	48.5
MoCo w/ masking	15.2	48.4
RCL	88.3	46.5

Masking as a Data Augmentation vs. RCL: In the reconstructive branch, RCL introduces masked input images. Some may wonder whether the improvements are coming from this

masking operation, since cutting out the input signals can be viewed as one way of augmentation (Chen et al. 2020a). However, here in Table 6, we show the performance of MoCo with and without masking augmentation on Colorful-MNIST (we use the same masking strategy as the reconstructive branch of RCL). As shown in the table, the performance of MoCo stays similar with or without masking augmentation. This demonstrate that the improvements of RCL do not come from this augmentation.

Table 7: Performance of RCL on Colorful-MNIST with and without warm-up training.

Warm-up Training	Colorful-MNIST	
	DIGIT CLS ACC. (%)	BKGD CLS ACC. (%)
No	24.9	47.8
Yes	88.3	46.5

Warm-up Training: To show the effectiveness of the proposed warm-up training strategy (Sec. 3 (c)), we compare the results of warm-up training with the results of directly using the combined loss \mathcal{L} (i.e., combining the reconstruction loss and the contrastive loss) from the beginning. As shown in Table 7, without the warm-up training, on Colorful-MNIST, RCL largely degenerates to become similar to the contrastive learning baselines and cannot learn good features related to digit classification. This indicates that without the warm-up phase, the contrastive loss can dominate the network causing it to learn the shortcut at the beginning, and that the network cannot later jump out of the local minimum associated with the shortcut. On the other hand, with warm-up training, the network first learns a coarse representation; then the contrastive loss helps the network learn more fine-grained representations.

Performance of RCL with different λ : In RCL, the combined loss is a weighted average of the reconstruction loss and the contrastive loss, i.e., $\mathcal{L} = \mathcal{L}_c + \lambda \cdot \mathcal{L}_r$. In the experiments of main paper, λ is set to 10. In this section, we investigate how different λ affects the performance of RCL. Note that when $\lambda = 0$, RCL degenerates to contrastive learning; when $\lambda \rightarrow \infty$, RCL degenerates to reconstructive learning.

Table 8 compares the performance of RCL with different λ . As we can see from the results, when $\lambda < 100$, with larger λ , the accuracy of the digit classification increases, while the accuracy of background classification decreases. Moreover, the λ values between 10 and 100 gives quite similar performances, indicating a balancing between contrastive loss and reconstruction loss. For $\lambda > 100$, the reconstruction loss dominates the contrastive loss and harm the performance. Therefore, we fix $\lambda = 10$ for all experiments.

Reconstructive Learning vs. RCL: In the main paper, we mainly compare RCL with contrastive learning since contrastive learning is the current unsupervised learning SOTA on ImageNet and outperforms reconstructive learning by a large margin (Chen et al. 2020a; Grill et al. 2020). Here, we also compare RCL with reconstructive learning on various

Table 8: Digit classification and background classification accuracy of RCL with different λ on Colorful-MNIST dataset.

λ	0	1	5	10	25	50	100	200	500	1000
DIGIT ACC (%)	15.7	48.6	69.8	88.3	88.2	88.3	88.1	87.5	86.3	85.0
BKGD ACC (%)	48.5	47.9	47.5	47.2	47.2	47.1	47.0	45.7	44.5	40.5

Table 9: Performance of RCL and reconstructive baselines on MPII for the downstream task of human pose estimation. \uparrow indicates the larger the value, the better the performance.

METRIC		Head \uparrow	Shoulder \uparrow	Elbow \uparrow	Wrist \uparrow	Hip \uparrow	Knee \uparrow	Ankle \uparrow	PCKh \uparrow
FIXED FEATURE EXTRACTOR	Inpainting	83.4	75.2	53.6	44.4	56.4	44.3	45.7	59.0
	Colorization	79.5	71.2	49.6	42.1	54.2	40.7	41.9	55.1
	Autoencoder	79.1	70.1	47.2	41.6	51.9	39.1	40.3	53.8
	RCL (ours)	85.7	78.8	61.7	51.3	64.4	55.6	49.2	65.1
	IMPROVEMENTS	+2.3	+3.6	+8.1	+6.9	+8.0	+11.3	+3.5	+6.1
FINE- TUNING	Inpainting	96.3	95.2	87.9	82.1	87.8	82.5	77.6	87.7
	Colorization	96.2	95.1	87.7	82.1	87.8	82.5	77.5	87.6
	Autoencoder	96.0	94.9	87.6	82.0	87.6	82.4	77.3	87.5
	RCL (ours)	96.3	94.9	88.1	82.3	87.9	82.8	77.8	87.8
	IMPROVEMENTS	+0.0	-0.3	+0.2	+0.2	+0.1	+0.3	+0.2	+0.1

Table 10: Performance on FairFace with RCL and different reconstructive unsupervised learning methods. The models are evaluated on downstream tasks of age, gender and ethnicity classification.

METRIC		AGE CLS ACC. (%)	GENDER CLS ACC. (%)	ETHN. CLS ACC. (%)
FIXED FEATURE EXTRACTOR	Inpainting	46.3	83.6	52.9
	Colorization	46.1	82.9	53.8
	Autoencoder	44.3	80.1	50.7
	RCL (ours)	50.0	87.2	61.2
	IMPROVEMENT	+3.7	+3.6	+7.4
FINE- TUNING	Inpainting	55.0	91.8	68.3
	Colorization	54.9	92.0	68.6
	Autoencoder	54.5	91.3	67.9
	RCL (ours)	55.3	92.3	69.0
	IMPROVEMENT	+0.3	+0.3	+0.4

Table 11: Performance on Colorful-MNIST under different methods. The models are evaluated on the downstream tasks of digit classification and background object classification.

METRIC		DIGIT CLS ACC. (%)	BKGD CLS ACC. (%)
FIXED FEATURE EXTRACTOR	Inpainting	84.7	35.0
	Colorization	80.7	38.4
	Autoencoder	81.0	32.9
	RCL (ours)	88.3	46.5
	IMPROVEMENT	+3.2	+8.1
FINE- TUNING	Inpainting	92.9	54.5
	Colorization	92.5	54.5
	Autoencoder	92.4	54.1
	RCL (ours)	93.3	54.7
	IMPROVEMENT	+0.4	+0.2

datasets to demonstrate the effectiveness of the contrastive branch of RCL. Tables [2-4] compare RCL with Inpainting (Pathak et al. 2016), Colorization (Zhang, Isola, and Efros 2016) and Auto-encoder on the RGB datasets. The results demonstrate that RCL outperforms all reconstructive learning baselines by a large margin. This is because the contrastive branch in RCL can significantly improve the quality of the learned representation so it can achieve much better performance on downstream tasks.

Appendix B: Additional Proofs

Here we formally prove Corollary 1 and 2.

Corollary 3. For any lifting operator \mathcal{T}_σ , if $\hat{Z} = \{\hat{z}_i\}$ is a stationary point of $\mathcal{E}_{\text{limNCE}}(Z; X, \tau, d_1)$, then $\mathcal{T}_\sigma(\hat{Z})$ is a stationary point of $\mathcal{E}_{\text{limNCE}}(Z; X, \tau, d_2)$.

Proof. The proof is in the supplemental material. \square

Proof. \hat{Z} is a stationary point of $\mathcal{E}_{\text{limNCE}}(Z; X, \tau, d_1)$ implies $\nabla_{z_i} \mathcal{E}_{\text{limNCE}}(\hat{Z}; X, \tau, d_1) = 0$. Therefore, by Lemma 2, $\nabla_{z_i} \mathcal{E}_{\text{limNCE}}(\mathcal{T}_\sigma(\hat{Z}); X, \tau, d_2) = \mathcal{T}_\sigma(\nabla_{z_i} \mathcal{E}_{\text{limNCE}}(\hat{Z}; X, \tau, d_1)) = 0$. \square

Corollary 4. For any lifting operator \mathcal{T}_σ , if $\hat{Z} = \{\hat{z}_i\}$ is a global minimum of $\mathcal{E}_{\text{limNCE}}(Z; X, \tau, d_1)$ with a positive definite Hessian matrix, then $\mathcal{T}_\sigma(\hat{Z})$ is a saddle point or a local minimum of $\mathcal{E}_{\text{limNCE}}(Z; X, \tau, d_2)$.

Proof. From Corollary 3, $\mathcal{T}_\sigma(\hat{Z})$ is a stationary point of $\mathcal{E}_{\text{limNCE}}(Z; X, \tau, d_2)$. Since the Hessian matrix of $\mathcal{E}_{\text{limNCE}}(Z; X, \tau, d_1)$ at \hat{Z} is positive definite, $\forall r > 0, \exists Z' \in$

$B_r(\hat{Z})$ s.t. $\mathcal{E}_{\text{limNCE}}(Z'; X, \tau, d_1) > \mathcal{E}_{\text{limNCE}}(Z; X, \tau, d_2)$, where $B_r(Z) = \{Z' \in \mathbb{S}^{d-1} \mid \|Z - Z'\|_2 < r\}$ is the neighborhood of Z with radius r . Therefore, $\mathcal{E}_{\text{limNCE}}(\mathcal{T}_\sigma(Z'); X, \tau, d_1) > \mathcal{E}_{\text{limNCE}}(\mathcal{T}_\sigma(Z); X, \tau, d_2)$ (Lemma 1). Note that $Z' \in B_r(\hat{Z}) \rightarrow \mathcal{T}_\sigma(Z') \in B_r(\mathcal{T}_\sigma(\hat{Z}))$. Therefore, $\forall r > 0, \exists \mathcal{T}_\sigma(Z') \in B_r(\mathcal{T}_\sigma(\hat{Z}))$ s.t. $\mathcal{E}_{\text{limNCE}}(\mathcal{T}_\sigma(Z'); X, \tau, d_1) > \mathcal{E}_{\text{limNCE}}(\mathcal{T}_\sigma(Z); X, \tau, d_2)$. Therefore, $\mathcal{T}_\sigma(\hat{Z})$ is not a local maximum, so it can only be a local minimum or a saddle point of $\mathcal{E}_{\text{limNCE}}(Z; X, \tau, d_2)$. \square

Appendix C: Implementation Details

In this section, we provide the implementation details of the models used in our experiments. All experiments are performed on 8 NVIDIA Titan X Pascal GPUs. On each dataset, we fix the batch size and training epochs for different baselines for a fair comparison. Other parameters for each baseline follow the original paper to optimize for its best performance. Code will also be released upon acceptance of the paper.

ImageNet: We use a standard ResNet-50 for the encoder network. The decoder network is a 11-layer deconvolutional network. The projection head for contrastive learning is a 2-layer non-linear head which embeds the feature into a 128-dimensional unit sphere. The same network structure is used for all baselines and RCL.

We follow the open repo of (Chen et al. 2020c) for the implementation of MoCo baselines and RCL on ImageNet. For results on SimCLR, we follow the results reported in (Grill et al. 2020). All baselines and RCL is trained for 800 epochs with a batch size of 256. For the reconstructive branch of RCL and the reconstructive baseline, we mask out 3 to 5 rectangles at random locations in the image. The size of each square is chosen by setting its side randomly between 40 and 80 pixels. For the contrastive branch of RCL, we apply the same training scheme as MoCo. The first 10 epochs are warm-up epochs, where we only train the network with the reconstruction loss \mathcal{L}_r . For later training, we set $\lambda = 10$. For other RGB datasets, we mainly follows similar implementation as ImageNet.

MPII: We use the network structure similar to the one in (Xiao, Wu, and Wei 2018). We use a ResNet-50 for the encoder network. Three deconvolutional layers with kernel size 4 and one convolutional layer with kernel size 1 is added on top of the encoded feature to transfer the feature into 13 heatmaps corresponding to 13 keypoints. For the contrastive branch, a 2-layer non-linear projection head is added on top of the encoded feature and embeds the feature into a 128-dimensional unit sphere. For the reconstructive branch, a decoder network similar to the pose estimation deconvolution network (only the number of output channels is changed to 3) is used to reconstruct the original image. Other implementation details are the same as ImageNet.

For the baselines and RCL, we train the network for 300 epochs with a batch size of 256. The data augmentation is the same as the baseline augmentations on ImageNet. For RCL, the first 10 epochs are warm-up epochs, where we only train the network with the reconstruction loss \mathcal{L}_r .

FairFace: We use a standard ResNet-50 for the encoder

network. The decoder network is a 11-layer deconvolutional network. The projection head for contrastive learning is a 2-layer non-linear head which embeds the feature into a 128-dimensional unit sphere. The same network structure is used for all baselines and RCL.

For the baselines and RCL, we train the network for 1000 epochs with a batch size of 256. The data augmentation is the same as the baseline augmentations on ImageNet. For RCL, the first 30 epochs are warm-up epochs, where we only train the network with the reconstruction loss \mathcal{L}_r .

Colorful-MNIST: We use a 6-layer ConvNet for the encoder. The encoder weights for the predictive and contrastive branches are shared. The decoder is a 6-layer deconvolutional network symmetric to the encoder. The projection head for contrastive learning is a 2-layer non-linear head which embeds the feature into a 64-dim normalized space.

We use the SGD optimizer with 0.1 learning rate, $1e-4$ weight decay, and 0.9 momentum to train the model for 200 epochs. The learning rate is scaled with a factor of 0.1 at epoch 150 and 175. The batch size is set to 512. The temperature for contrastive loss is set to 0.1. For RCL, the first 30 epochs are warm-up epochs, where we only train the network with the reconstruction loss \mathcal{L}_r .

For RCL, for each input image after augmentation with a size of 64 by 64 pixels, we randomly mask out 3 to 5 rectangle patches at random locations in the image and fill them with the average pixel value of the dataset. The size of each square is chosen by setting its side randomly between 10 and 16 pixels.

Appendix D: Experiments' Setup and Evaluation Metrics

Setup. On ImageNet, as common in the literature, we evaluate the representations with the encoder fixed and only the linear classifier is trained. On all other datasets, we evaluate the representations under two different settings: fixed feature encoder setting and fine-tuning setting. In the fixed feature encoder setting, the ResNet encoder is fixed and only the classifier (FairFace, Colorful-MNIST) or the 4-layer decoder network (MPII); In the fine-tuning setting, the encoder is initialized with the pre-trained model and fine-tuned during training.

Evaluation Metrics. For ImageNet, FairFace and Colorful-MNIST, the evaluation metrics are the standard Top-1 classification accuracy. For MPPII, we evaluate the learned representations under the single pose estimation setting (Andriluka et al. 2014). Each person is cropped using the approximate location and scale provided by the dataset. Similar to prior works, we report the PCKh (Percentage of Correct Keypoints that uses the matching threshold as 50% of the head segment length) value of each keypoint and an overall weighted averaged PCKh over all keypoints (head, shoulder, elbow, wrist, hip, knee, ankle).